DESIGN OF LEARNING INPUT SHAPING TECHNIQUE FOR SUPPRESSING RESIDUAL VIBRATIONS IN AN INDUSTRIAL ROBOT

Juyi Park,* Pyung-Hun Chang,* and Hyung-Soon Park *

** Korea Advanced Institute of Science and Technology, 373-1, Yusong-gu, Taejon, 305-701, Korea*

Abstract: In this paper, a practical solution for suppressing residual vibrations of industrial robots is proposed. For suppressing the nonlinear and time-varying vibrations, we adopt learning input shaping technique (LIST), which is suitable for robots doing repetitive tasks. Through theoretical analyses and experiments, it is established that we can treat the MIMO dynamics of a robot as a set of decoupled SISO dynamics, making the application of LIST very practical. LIST is applied to a 6 DOF industrial robot intended for handling heavy payloads(up to 120 Kg) and experimented for both point-to-point motion and continuous path motion. Experimental results show that LIST can suppress residual vibrations to a level similar to that of time-varying input shaping technique, a much more sophisticated method, thereby demonstrating its potential for suppressing the residual vibrations in industrial robots.

1. INTRODUCTION

In controlling industrial robots, fast and precise motions are required for better productivity. Such motions, however, are often restricted by the residual vibrations in the end-effector, which tend to be time-varying and nonlinear owing to the configuration-dependent inertia-variation and the nonlinear stiffness of the gears.

For suppressing residual vibrations in flexible systems, there are two distinct approaches: open-loop feedforward (Aspinwall, 1980) and closed-loop feedback(Kotnik *et al.*, 1988). In terms of performance, the latter scheme is more attractive than the former, because it is inherently the more robust against disturbances and parameter variations. In terms of practical implementation, however, the closed-loop approach makes overall systems the more complex, expensive, and difficult to control. More specifically, the increased states due to vibration modes increase the order of the control laws, thereby requiring more computation and more sensors as well as the measurability of the additional states. Because of this difficulty, many researchers have studied feedforward schemes combined with feedback controllers(Singer and Seering, 1990; Meckl and Seering, 1988). They reported that the scheme is simple in its structure and robust against disturbances or parameter variations, so that it is very useful for practical applications.

Based on the observations above, we have considered the input shaping technique (IST), proposed by Singer(Singer and Seering, 1990), as the feedforward scheme to be combined with a feedback controller. Since first proposed, the IST has attracted attentions owing to its effectiveness and simplicity. Its effectiveness has been confirmed by the application results from practical systems such as a surface mounting machine(Park and Chang, 1996), a single link flexible spacecraft(Liu and Wie, 1992), and an open container of liquid(Feddema *et al.*, 1997). Nevertheless, since the IST was proposed originally for linear time-invariant systems(Singer and Seering, 1990), it is not so effective for systems with nonlinearity and time-varying characteristics, such as multi-links robots we are concerned with. Even robust IST(Singer and Seering, 1990), which handles inaccuracy of frequency estimation, is not of much help for these systems.

In response to this difficulty, there have been many studies to improve IST for nonlinear and time-varying systems. As for non-robotic systems, there are on-line adaptive schemes by Tzes and Yurkovich(Tzes and Yurkovich, 1993) and Bodson(Bodson, 1997), respectively. As for robotic systems, Rappole(Rappole, 1992) applied time-varying input shaping technique (TVIST) to a two-link flexible manipulator using a look-up table, Magee and Book(Magee and Book, 1993) modified the IST to eliminate the first two modes of vibration in a large and flexible manipulator having configuration-dependent inertia. Cho and Park(Cho and Park, 1995) proposed a method for determining the exact time-varying impulse sequence, and applied it to a two-link flexible robot. Besides, there have been similar attempts to apply the IST to various robots(Khorrami and Jain, 1992).

But these schemes require intensive computing power for real time computation, or memory space for a frequency-map. Moreover, some schemes require an exact dynamic model of plant. Further, the robots controlled in this previous research are mostly laboratory-level robots for research purposes, and few of them to our knowledge can be regarded as industrial robots. These robots tend to have either really flexible links or overly flexible joints, hence possessing dominant flexibility that is easy to locate and model. An industrial robot, on the other hand, not having such dominant flexibility, its identification itself poses substantial difficulties, not to mention its cause.

The IST we have adopted in this paper is the learning input shaping technique (LIST)(Park and Chang, 1998), which *iteratively* updates the parameters of IST from previous trials. The idea central to this approach came from our observation that most application situations of industrial robots are *planned* in advance and the required tasks are *repetitive* in nature. The robot to which we apply LIST is a

Table 1. Description and numerical values for parameters

parameter	description	value
l_a, l_c	length of link a, link c	1.25 $[m]$
l_b	length of link b	0.5 $[m]$
l_d	length of link d	1.8 $[m]$
m_a	mass of link a	160.0 $[kg]$
m_b	mass of link b	260.0 $[kg]$
m_c	mass of link c	30.0 $[kg]$
m_d	mass of link d	260.0 $[kg]$

real industrial robot intended for handling heavy payloads. Through some theoretical analyses and experiments, it is established that we can treat the MIMO dynamics of a robot as a set of decoupled SISO dynamics, making the application of LIST very practical. Then, we use the input/output value for progressing the learning process, so that its nonlinear and time-varying residual vibrations can be suppressed without a dynamic model of the robot. Then the experimental results of LIST are compared to those of TVIST so that merits and demerits of them can be evaluated. This procedure can be a useful guideline for various industrial robots other than ours.

This paper is organized as follows: the following section presents the dynamic properties of the industrial robot, showing both nonlinear as well as time-varying vibrations for the robot. In Section 3, the main idea and the algorithm of LIST is presented. Section 4 describes our experimental results, and is followed in section 5 with conclusions.

2. DYNAMIC PROPERTIES OF THE ROBOT

In this section, the dynamic properties of the robot is described in order to show the nonlinear and time-varying characteristics of the robot.

The industrial robot of our concern has a parallelogram-linkage structure with 6 degrees of freedom, the schematic diagram of which is shown in figure 1. Both the description and the approximate values for the parameters in figure 1 are presented in Table 1. As can be expected from the numerical values of these parameters, the robot is intended for handling heavy payloads or spot-welding, the maximum payload of which is designed to be 120 kg.

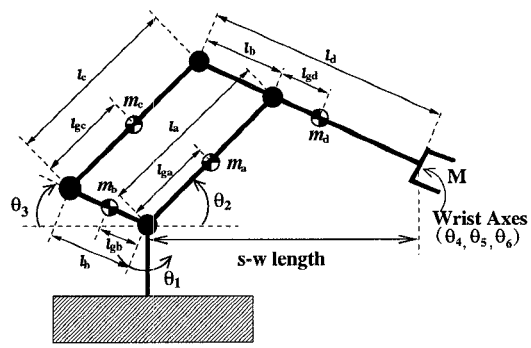

Fig. 1. The schematic diagram for the industrial robot.

To examine its frequency variation properties, the dynamic equation for the robot was derived based on the schematic diagram depicted in figure 1. As shown in figure 1, the first axis, specified as the joint axis for θ_1, is the swing-axis, which rotates the overall linkage. The vertical axes, denoted as θ_2 and θ_3, determine the configuration of the parallelogram linkage. The last three axes, denoted as θ_4, θ_5, and θ_6, determine the orientation of the end-effector. Note that these last three axes have little effect on the inertia-variation and thus on the frequency-variation; therefore, the dynamic equation is derived only for the first three joints.

Since joint flexibility is considered as the primary source for robot vibration, it is included in the model. The flexibility of the i-th joint is modeled as a torsional spring with stiffness, K_{Ti} (Kinceler and Meckl, 1996). Consequently, each axis also includes two joint variables representing both motor angle (θ_{mi}) and link angle (θ_i), as shown in figure 2.

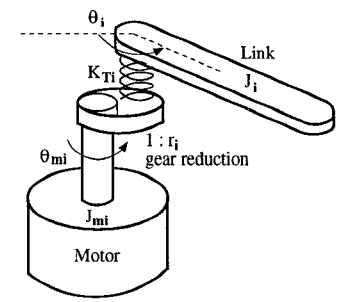

Fig. 2. The model of joint flexibility.

The dynamic equation for this robot is derived by using Lagrange's method and expressed as follows:

$$M_{11}\ddot{\theta}_{m1} + b_{m1}\dot{\theta}_{m1} + \frac{b_{k1}}{r_1}\dot{\theta}_{r1} + \frac{K_{T1}}{r_1}\theta_{r1} = \tau_1 \quad (1)$$

$$M_{22}\ddot{\theta}_1 + b_1\dot{\theta}_1 - b_{k1}\dot{\theta}_{r1} - K_{T1}\theta_{r1} + N_1(\boldsymbol{\theta}, \dot{\boldsymbol{\theta}}) = 0 \quad (2)$$

$$M_{33}\ddot{\theta}_{m2} + b_{m2}\dot{\theta}_{m2} + \frac{b_{k2}}{r_2}\dot{\theta}_{r2} + \frac{K_{T2}}{r_2}\theta_{r2} = \tau_2 \quad (3)$$

$$M_{44}\ddot{\theta}_2 + M_{46}\ddot{\theta}_3 + b_2\dot{\theta}_2 - b_{k2}\dot{\theta}_{r2} - K_{T2}\theta_{r2} + N_2(\boldsymbol{\theta}, \dot{\boldsymbol{\theta}}) + G_2(\boldsymbol{\theta}) = 0 \quad (4)$$

$$M_{55}\ddot{\theta}_{m3} + b_{m3}\dot{\theta}_{m3} + \frac{b_{k3}}{r_3}\dot{\theta}_{r3} + \frac{K_{T3}}{r_3}\theta_{r3} = \tau_3 \quad (5)$$

$$M_{64}\ddot{\theta}_2 + M_{66}\ddot{\theta}_3 + b_3\dot{\theta}_3 - b_{k3}\dot{\theta}_{r3} - K_{T3} - \theta_{r3} + N_3(\boldsymbol{\theta}, \dot{\boldsymbol{\theta}}) + G_3(\boldsymbol{\theta}) = 0, \quad (6)$$

where $\theta_{ri} = \left(\frac{\theta_{mi}}{r_i} - \theta_i\right)$, $\boldsymbol{\theta} = [\theta_1 \quad \theta_2 \quad \theta_3]^T$; and $N_i(\boldsymbol{\theta}, \dot{\boldsymbol{\theta}})$ denotes the Coriolis and centrifugal torque and $G_i(\boldsymbol{\theta})$ the gravity torque, at the i-th joint. In the equations above, it is assumed that viscous damping with a coefficient of b_{mi} is also present at each motor, b_i at each joint, and b_{ki} at each torsional spring.

Under the assumption that each link has a uniform and symmetric cross-section, the elements of $M_{ij}(\boldsymbol{\theta})$'s can be expressed as the following.

$$M_{11} = J_{m1} \quad (7)$$

$$M_{22} = (m_a l_{ga}^2 + J_a + J_c)c_2^2 + (m_b l_{gb}^2 + J_b + J_d)c_3^2 + m_c(l_b c_3 - l_{gc} c_2)^2 + m_d(l_c c_2 + l_{gd} c_3)^2 + m_P\{l_c c_2 + (l_d - l_b)c_3\}^2 \quad (8)$$

$$M_{33} = J_{m2} \quad (9)$$

$$M_{44} = m_a l_{ga}^2 + J_a + m_c l_{gc}^2 + J_c + m_d l_a^2 + m_P l_a^2 \quad (10)$$

$$M_{46} = \{m_d l_a l_{gd} - m_c l_b l_{gc} + m_P l_a (l_d - l_b)\}\cos(\theta_2 - \theta_3) \quad (11)$$

$$M_{64} = M_{46} \quad (12)$$

$$M_{55} = J_{m3} \quad (13)$$

$$M_{66} = m_b l_{gb}^2 + J_b + m_c l_b^2 + m_d l_{gd}^2 + J_d + m_P(l_d - l_b)^2 \quad (14)$$

where l_k and l_{gk} $(k = a, b, c, d)$, as shown in figure 1, denote the length of the corresponding link, and the length to the center of gravity, respectively. In the same manner, m_k and J_k represent the mass of the link and the moment of inertia, respectively. In addition, m_P denotes

the payload, which is attached at the end-effector, and c_i and s_i symbolize $\cos\theta_i$ and $\sin\theta_i$, respectively.

Note in equation (8) that the inertia about the swing-axis, M_{22}, varies with both θ_2 and θ_3, whereas M_{44} and M_{66} have constant values in equation (10) and (14). Furthermore, M_{44} and M_{66} take smaller values as compared to M_{22}, and so does the magnitude of the vibration. So, this observation implies that the *time-varying* residual vibration of the end effector is predominantly determined by that of the swing-axis. Practically, this finding is very important, because it enables us to concentrate on the swing-axis only. For the rest of the other axes, we can design other filters such as conventional IST, as if the residual vibrations were time-invariant.

In addition, the nonlinear functions, $N_i(\boldsymbol{\theta}, \dot{\boldsymbol{\theta}})$'s, cause the nonlinear residual vibration of the robot. Moreover, the nonlinear vibration appears to be further complicated by some mechanical properties of the robot, such as the nonlinear flexibility of the harmonic drive.

Owing to such time-varying and nonlinear characteristics, the residual vibration of the industrial robot is not well suppressed by conventional IST, which was derived for linear time invariant (LTI) systems.

3. ITERATIVE LEARNING INPUT SHAPING TECHNIQUE

To suppress the time-varying and nonlinear residual vibrations described in the previous chapter, learning input shaping technique (LIST) was applied to the industrial robot. This section presents its main idea and the algorithm for LIST.

3.1 *IST and measures representing residual vibrations*

The two-impulse sequence for suppressing the residual vibration is generally given in following form:

$$u(s) = \left[A_1 e^{-T_1 s} + A_2 e^{-T_2 s}\right] r(s) \qquad (15)$$

where $r(s)$ is the reference command. Clearly the two-impulse sequence has four parameters: the magnitudes of impulses A_1 and A_2, and the applying times T_1 and T_2. Without loss of generality, T_1 may be fixed to 0 for a faster response, and A_2 may also be fixed to $(1 - A_1)$ in order to maintain a unity gain. Then, there remain only two independent parameters to be determined, which are A_1 and T_2.

According to the study by Singer and Seering(Singer and Seering, 1990), the residual vibrations due to the two-impulse sequence vanishes if A_1 and T_2 are properly selected by following equations:

$$A_{1n} = \frac{1}{1 + e^{-\zeta\pi/\sqrt{1-\zeta^2}}} \qquad (16)$$

$$T_{2n} = \frac{\pi}{\omega_n \sqrt{1-\zeta^2}}\ , \qquad (17)$$

where $(\cdot)_n$ denotes the proper values of $(\cdot)$, and ζ, ω_n mean the damping ratio and the natural frequency of the residual vibration to be suppressed, respectively.

When $A_1 \neq A_{1n}$ or $T_2 \neq T_{2n}$, however, the residual vibration does not vanish after T_2. Depending on the combinations of the following two conditions, there are nine possible cases listed in Table 2, where ϕ denotes the phase differences between the residual vibrations with and without IST.

- **Condition 1 :** $A_1 > A_{1n}$ or $A_1 = A_{1n}$ or $A_1 < A_{1n}$
- **Condition 2 :** $T_2 > T_{2n}$ or $T_2 = T_{2n}$ or $T_2 < T_{2n}$

Table 2. The ranges of ϕ for nine possible cases.

	$A_1 > A_{1n}$	$A_1 = A_{1n}$	$A_1 < A_{1n}$
$T_2 > T_{2n}$	$0 < \phi < \frac{\pi}{2}$	$0 < \phi < \frac{\pi}{2}$	$0 < \phi < \pi$
$T_2 = T_{2n}$	$\phi = 0$	*no vib.*	$\phi = \pi$
$T_2 < T_{2n}$	$-\frac{\pi}{2} < \phi < 0$	$-\frac{\pi}{2} < \phi < 0$	$-\pi < \phi < 0$

Among the nine cases, two cases are selected to examine the responses: $A_1 = A_{1n}$ and $T_2 > T_{2n}$; and $A_1 = A_{1n}$ and $T_2 < T_{2n}$. figure 3 shows the responses to the two-impulse sequence, with the parameters from the above two cases. In the figure, the solid lines represent the original vibration, the unit impulse response without IST, and the dotted lines represent the resultant responses to the two-impulse sequence. The upper plot shows the response for the case $T_2 > T_{2n}$, and the lower plot for the case $T_2 < T_{2n}$. Both of the responses display that the residual vibrations still persist, and that phase differences also exist from the vibration without IST.

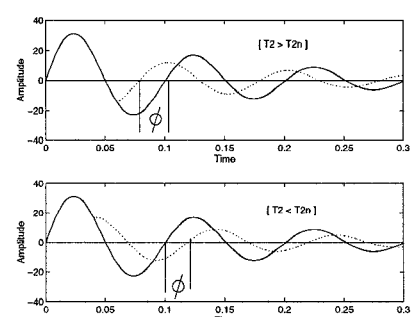

Fig. 3. The responses to the 2-impulse sequence with inaccurate parameters. Solid lines represent unit impulse responses; dotted lines represent the resultant responses to the 2-impulse sequence with a large (upper plot) or a small (lower plot) T_2.

In adopting a learning scheme for IST, we have used two measures: the magnitude of residual vibration and the phase difference mentioned above. More specifically, the magnitude measure M is defined as

$$M \equiv \int_{t_i}^{t_f} |\nu(t)| dt, \qquad (18)$$

where $\nu(t)$ is any signal representing residual vibration such as position, velocity, or acceleration. $t_i \leq t \leq t_f$ is the duration when the residual vibration is significant.

Another measure, ϕ, is the phase difference between the residual vibration with and without IST. Examples of ϕ are shown for improper sets of T_2 in figure 3. When T_2 is larger than the proper value, ϕ has a positive value or phase lead in the upper plot. On the other hand, when T_2 is smaller than the proper value, ϕ then has a negative value or phase lag in the lower plot. Hence, by observing ϕ, one can determine whether an IST parameter is larger or smaller than the proper value.

3.2 *Iterative learning scheme*

The iterative learning scheme updates the IST parameters, A_1 and T_2, by using the results from previous trials.

Specifically, M and ϕ are obtained from the previous results, and then the IST parameters are updated to further minimize M. The overall algorithm for this is illustrated by a flow-chart in figure4, and also summarized as follows:

- **Step 1 :** Select an initial guess for A_1 and T_2, and then obtain residual vibration, either by simulation or experiment.
- **Step 2 :** Fix A_1. Continue to simulate (or experiment), while varying T_2, until M has a minimum value.
- **Step 3 :** Set the best T_2 obtained at Step 2 fixed, and then repeat the same procedure for updating A_1.
- **Step 4 :** Repeat steps 2 and 3 until M has a minimum value.

The initial guesses of A_1 and T_2 are determined by (16) and (17) from our observations of the residual vibrations without IST. Yet, for nonlinear and time-varying systems, these initial guesses are usually insufficient in suppressing the residual vibrations. Hence, a learning process is also required to obtain the proper values for the IST parameters.

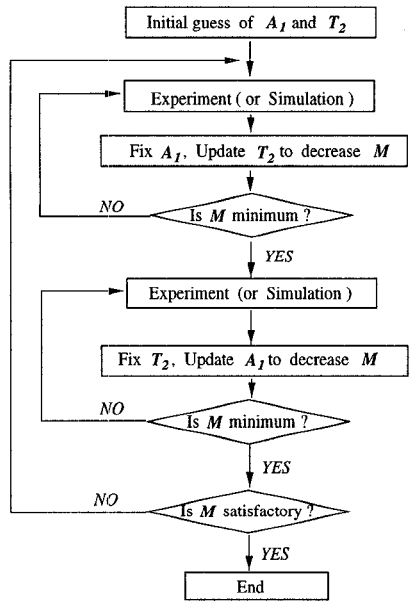

Fig. 4. The flow-chart of Learning Input Shaping Technique (LIST).

In the proposed learning scheme, parameters are updated by using both their values and their corresponding M from the previous two trials. Regarding the previous two trials, we have two different convergent situations, as illustrated in figures 5 (a) and (b), respectively.

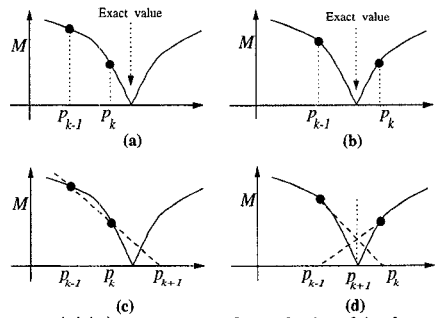

Fig. 5. The (a)(b) represent the relationship between of two parameters which were used in previous trials, and the (c)(d) represent the updating rules for the each case.

The two situations require two different updating rules as follows:

- When both of the two values are either larger or smaller than the most exact value, as shown in figure 5(a), the secant method, which is a root finding method, is then used for the next trial. This updating rule is illustrated in figure 5(c), and also formulated in the following equation.

$$p_{k+1} = \frac{M_{k-1}}{M_{k-1} - M_k}(p_k - p_{k-1}) + p_{k-1}, \quad (19)$$

  where the M_j and the p_j mean the M and the parameter, A_1 or T_2, of the jth trial, respectively.
- When one of the values is larger than the exact value, while the other smaller, as seen in figure 5(b), the weighted average value of the two parameters is then used for the next trial(figure 5(d)), as follows:

$$p_{k+1} = \frac{M_{k-1}p_k + M_k p_{k-1}}{M_{k-1} + M_k}. \quad (20)$$

With regard to this procedure, it is therefore very important to discern which of the two above situations we are in. For both LTI systems or nonlinear time-varying systems having phase characteristics similar to those of LTI systems, we can easily do so by observing the value of ϕ, as described in Table 2.

For some nonlinear systems that have different phase characteristics, however, this phase information is not reliable any more. For instance, a nonlinear mass-spring system can vibrate with a decreasing frequency at smaller amplitudes. The phase difference in this case is meaningless, because vibrations in comparison have different frequencies. Obviously, we need to also use the updating rules that do not demand phase information.

This end can be met by a simple trial-error method described as follows. An initial assumption is made that both the values of the parameters are either larger or smaller than the exact value, as in figure 5(a). Sometimes, the use of ϕ at this stage is helpful for the convergence of iteration. Under this assumption, we first calculate p_{k+1} by using the equation (19), and then obtain M_{k+1} through either the experiment or simulation using this p_{k+1}. If the M_{k+1} is smaller than M_k as assumed, the learning process further proceeds to the next cycle. On the other hand, M_{k+1} larger than M_k, as shown in figure 6, indicates that the p_{k+1} was not properly updated. In such a case, the p_{k+1} is then recalculated by using the equation (20). This trial-error method therefore clearly enables a proper updating of p_{k+1} without using phase information.

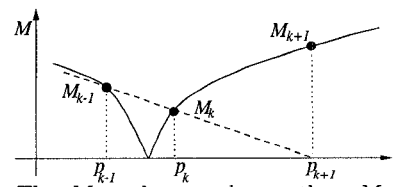

Fig. 6. The M_{k+1} become larger than M_k when the parameter is updated improperly.

4. EXPERIMENT

4.1 *Experimental Setup*

Experiments were performed to verify that LIST is effective for suppressing the residual vibrations in a robot

conducting repetitive tasks. For this, two types of reference trajectories were given, and the results from LIST were then compared to those of both conventional IST as well as TVIST based on Rappole's method(Rappole, 1992).

The schematic diagram of experimental setup is shown in figure 7. P-controllers that have inner PI velocity control loops are used as the position controllers. An accelerometer is attached at the tip of the robot, in order to measure the residual vibrations from the tip.

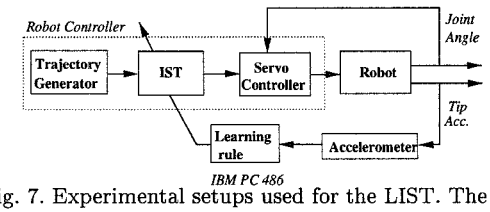

Fig. 7. Experimental setups used for the LIST. The learning process is done on the IBM-PC 486.

As shown in figure 7, IST is implemented on the robot controller, whereas the learning algorithm is carried out on an outside controller, IBM PC 486DX2-66. While the robot is moving, the acceleration signals sensed by the accelerometer are sent to the PC. Then the signals are filtered with a band-pass filter in order to filter out both drift signals and noise, and then it is stored in the memory of the PC. After 1-cycle of motion, the PC calculates M and ϕ, and then updates the IST parameters. Then the values of the IST parameters that are updated above are sent to the robot controller, and the next cycle follows.

Of the two different types of reference trajectories, the first type is designed for point-to-point motions so as to have trapezoidal velocity profiles; the second type is the same as the first one, except that it includes an intermediate via point to pass through with non-stop motion. It is well known that these trajectories are very often used in industrial applications. The joint angles of the points for designed trajectories are listed in Table 3.

Table 3. The joint angles of the points for designed trajectories.

	Initial point	Via point	Final point
Trajectory 1			
θ_1	0°	–	0°
θ_2	90°	–	57°
θ_3	0°	–	36°
Trajectory 2			
θ_1	58.6°	0°	−45°
θ_2	26°	90°	132°
θ_3	0°	0°	14°

Before applying IST filters to the robot, we examined the level of the residual vibrations without IST filters. figure 8 shows the tip acceleration signal through a filter with a bandwidth between 2Hz and 30Hz, when only a feedback control is used. Clearly, the residual vibrations without IST are substantial and problematic. Note that the robot is moving for 1.0s, the tip acceleration *after* 1.0s is regarded as the residual vibration.

Through the above experiment, we observed that the frequency of residual vibration decreases at smaller amplitude whereas the damping ratio remains nearly constant. The frequency variation, in our study, is caused by both the time-varying inertia coming from both a change in the robot's configuration as well as a nonlinear flexibility in the harmonic drive.

In order to suppress such vibrations, in addition to LIST, two other schemes of IST have been adopted: conventional

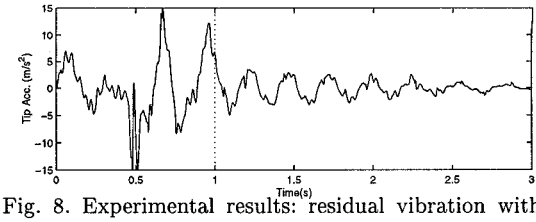

Fig. 8. Experimental results: residual vibration without IST. Note that because the robot moved for 1.0s, the tip acceleration after 1.0s is the residual vibration.

IST and the TVIST based on Rappole's method(Rappole, 1992), respectively, the details of which are described as follows:

- **Conventional IST :** For adopting conventional IST to nonlinear time-varying systems, we have designed an IST filter using the mean value of varying frequencies.
- **TVIST :** The TVIST is represented by:

$$u(t) = A_1 r(t) + A_2 r(t - T_2(t)). \qquad (21)$$

The applying time of a second impulse, $T_2(t)$, which varies with time, is estimated in real-time from the position data of each axis.

4.2 *Experimental Results*

figure 9 shows the experimental results for the first type of trajectories, which does not include via points. With the parameters chosen initially, the magnitude of the residual vibration is quite large. Yet, as the number of iterations increases, the residual vibrations become smaller. The decrease in residual vibrations shows itself in the plot of M vs. iteration numbers in figure 10.

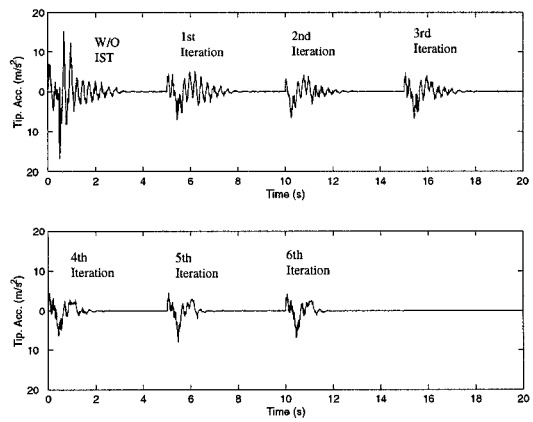

Fig. 9. Experimental results: the change in residual vibrations. Residual vibrations become smaller and smaller as the number of iterations increases.

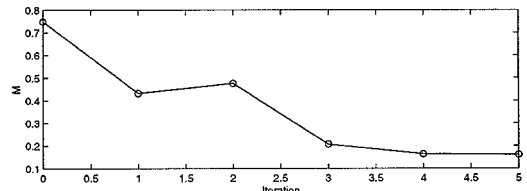

Fig. 10. Experimental results: the M decreases as the number of iterations increases.

In figure 11, the results from LIST are compared with those from TVIST. The comparison displays that both LIST and TVIST have well suppressed the residual vibrations,

which implies that we can choose one between the two schemes according to application conditions. If the real-time estimation of the varying frequency is both possible and affordable, TVIST is applicable; if not, yet the task is repeatable, LIST is suitable.

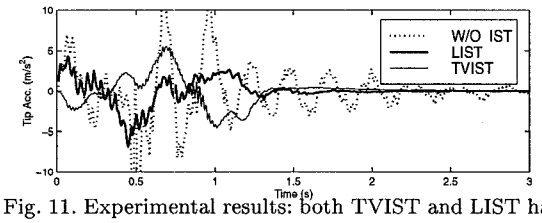

Fig. 11. Experimental results: both TVIST and LIST have suppressed the residual vibrations.

The experimental results for the second type of trajectories, including a via point are shown in figure 12 and figure 13. Similarly to the results for the first type of trajectories, LIST decreases the residual vibrations as the iteration goes on except for the 3rd iteration. On the 3rd iteration, M increases because of an improperly estimated ϕ, as illustrated in figure 6. Moreover, owing to another vibration mode of 25Hz shown in figure 13 (notably between 1.75s and 2.25s), M does not converge to zero. The experimental results in figure 13, however, show that the vibrations at 3.5Hz have virtually disappeared, as intended.

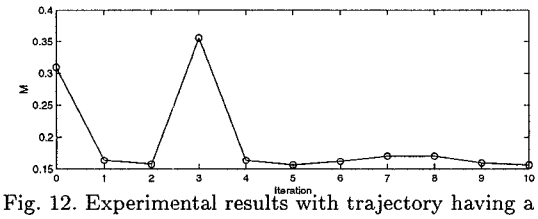

Fig. 12. Experimental results with trajectory having a via point: the M decreases as the number of iterations increases. An increasing of M at the 3rd iteration was caused by an improperly estimated ϕ.

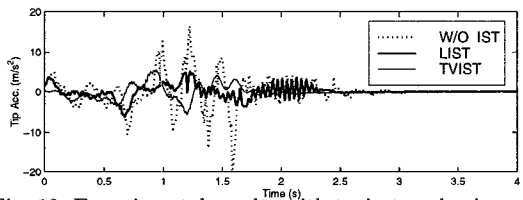

Fig. 13. Experimental results with trajectory having a via point: both TVIST and LIST have suppressed the residual vibrations.

From the results, we have concluded that LIST is suitable for suppressing the residual vibrations in a robot which is used for repetitive tasks.

5. CONCLUSIONS

For suppressing nonlinear and time-varying residual vibrations in a 6 degrees of freedom industrial robot, we have used LIST which updates the parameters of IST from previous trials.

After defining a set of measures for iteration, we have then used the input/output value for progressing the learning process, so that the residual vibrations could be suppressed without using a dynamic model.

Additionally, for simple and easy use of LIST, we have treated the MIMO dynamics of the robot as a set of decoupled SISO dynamics, based on theoretical analysis and experiments. As a result, application of LIST could be very simple and easy, because the iterative learning scheme has been used only at the swing axis.

In some experiments, LIST has suppressed the nonlinear and time-varying residual vibrations in the robot as well as time-varying IST (TVIST), which changes the IST parameters in real time according to an estimated frequency. Thus, we have concluded that LIST is suitable for suppressing the residual vibrations in industrial robots that are conducting repetitive tasks. Therefore, this result could serve a useful guideline for various industrial robots other than ours.

6. REFERENCES

Aspinwall, D. M. (1980). Acceleration profiles for minimizing residual response. *ASME Journal of Dynamic Systems, Measurement, and Control* **102**, 3–6.

Bodson, M. (1997). An adaptive algorithm for the tuning of two input shaping methods. *ACC* **3**, 1340–1344.

Cho, J. K. and Y. Park (1995). Vibration reduction in flexible systems using a time-varying impulse sequence. *Robotica* **13**, 305–313.

Feddema, J., C. Dohrmann and et al. (1997). A comparison of maneuver optimization and input shaping filters for robotically controlled slosh-free motion of an open container of liquid. *ACC.*

Hillsley, K. L. and S. Yurkovich (1991). Vibration control of a two-link flexible robot arm. *IEEE ICRA* pp. 2121–2126.

Khorrami, F. and S. Jain (1992). Experimental results on an inner/outer loop controller for a two-link flexible manipulator. *IEEE ICRA* pp. 742–747.

Kinceler, R. and P. H. Meckl (1996). Corrective input shaping for a flexible-joint manipulator performing point-to-point motion. *IEEE ICRA* pp. 391–396.

Kotnik, P. T., S. Yurkovich and U. Ozguner (1988). Acceleration feedback for control of a flexible manipulator arm. *J. of Robotics Systems* **5**(3), 181–196.

Liu, Q. and B. Wie (1992). Robust time-optimal control of uncertain flexible spacecraft. *J. of Guidance and Control* **15**, 597–604.

Magee, D. P. and W. J. Book (1993). Implementing modified command filtering to eliminate multiple modes of vibration. *ACC* pp. 2700–2704.

Meckl, P. H. and W. P. Seering (1988). Controlling velocity-limited systems to reduce residual vibration. *IEEE ICRA.*

Park, J. and P. H. Chang (1996). Use of input shaping technique with a robust feedback control and its application to the position control of surface mount machine. *IEEE CCA* pp. 397–402.

Park, J. and P.H. Chang (1998). Learning input shaping technique for non-lti systems. *ACC.*

Rappole, B. W. (1992). *Minimizing Residual Vibrations in Flexible Systems.* Master thesis, Department of Mechanical Engineering, MIT.

Singer, N. C. and W. P. Seering (1990). Preshaping command inputs to reduce system vibration. *ASME Journal of Dynamic Systems, Measurement, and Control* **112**, 76–82.

Tzes, A. and S. Yurkovich (1993). An adaptive input shaping control scheme for vibration suppression in slewing flexible structures. *IEEE Transactions on Control Systems Technology* **1**, 114–121.